

### **3. SYNTHESIS OF RESULTS: LOGGING WHILE DRILLING, NORTHERN BARBADOS ACCRETIONARY PRISM<sup>1</sup>**

J. Casey Moore<sup>2</sup>

#### **ABSTRACT**

Leg 171A collected logging while drilling (LWD) data at three sites in the northern Barbados accretionary prism and two in the section just seaward of the prism. These borehole logs, plus extensive information from previous Deep Sea Drilling Project and Ocean Drilling Program legs and a three-dimensional (3-D) seismic survey, provide new insights on the evolution of this accretionary prism.

Application of multivariate statistical methods to the LWD data quickly, reliably, and objectively define logging units that correlate well with the lithologic units from cored holes. Calculation of resistivity-based porosities allowed estimation of borehole velocities that were not directly measured by the LWD tools.

LWD data combined with previous coring results indicate that a low-density radiolarian claystone characterizes the proto-décollement zone, facilitates normal faulting in the incoming section, and localizes the décollement zone beneath the accretionary prism. Site 1045 data indicate that a low-density interval also characterizes the strong negative-polarity seismic reflections from the décollement zone. Both the individual LWD sites and an inversion of the 3-D seismic data for density indicate that the low-density décollement zone progressively consolidates with underthrusting. A northeasterly trending band of negative-polarity reflections in the décollement zone is an exception to this progressive densification process and shows anomalously low density caused by an arrested consolidation. Fluid flow from depth may account for the arrested consolidation of the northeasterly band of anomalously low density. Densification of the décollement zone is caused primarily by

<sup>1</sup>Moore, J.C., 2000. Synthesis of results: logging while drilling, northern Barbados accretionary prism. *In* Moore, J.C., and Klaus, A. (Eds.), *Proc. ODP, Sci. Results*, 171A, 1–25 [Online]. Available from World Wide Web: <[http://www-odp.tamu.edu/publications/171A\\_SR/VOLUME/CHAPTERS/SR171A03.PDF](http://www-odp.tamu.edu/publications/171A_SR/VOLUME/CHAPTERS/SR171A03.PDF)>. [Cited YYYY-MM-DD]

<sup>2</sup>Earth Sciences, University of California at Santa Cruz, Santa Cruz CA 95064, USA. [cmoore@es.ucsc.edu](mailto:cmoore@es.ucsc.edu)

Initial receipt: 14 December 1999

Acceptance: 7 July 2000

Web publication: 2 October 2000

Ms 171ASR-101

collapse of pore spaces between clay minerals and secondarily by collapse of radiolarian porosity, mineral phase changes, and zeolite precipitation. Previous coring results and, arguably, the seismic reflection data indicate that the décollement remains localized in an interval of low-density radiolarian claystone. Weakening of this smectite-rich lithology during shear explains the tendency of the décollement to remain localized in its initial position. An inadvertent two-hole hydrologic test conducted during LWD operations indicates significantly higher permeability over the scale of 50 m than that inferred previously from single borehole tests.

## INTRODUCTION

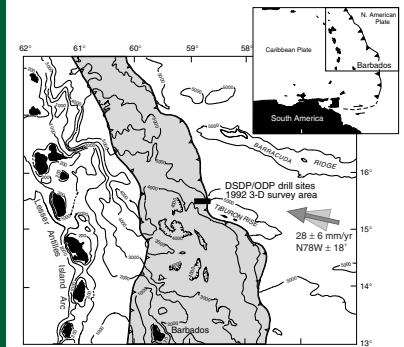
Leg 171A focused on the role of fluids in deformation along the subduction megathrust between the North American and Caribbean plates (Fig. F1) in the northern Barbados Ridge area. Previously, Deep Sea Drilling Project (DSDP) Leg 78A and Ocean Drilling Program (ODP) Legs 110 and 156 drilled in this region, with good core recovery and successful installation of borehole instrumentation (Biju-Duval and Moore, 1984; Masclé, Moore, Taylor, et al., 1988; Shipley, Ogawa, Blum, et al., 1995). Repeated attempts at wireline logging during previous DSDP and ODP legs produced limited physical properties data of poor quality and justified the application of logging while drilling (LWD) in this environment. After a successful test of LWD tools during ODP Leg 156, we applied LWD technology during Leg 171A to acquire a comprehensive suite of borehole logs to better interpret the extensive seismic and drilling results. The Leg 171A drilling results complement a high-quality three-dimensional (3-D) seismic survey and provide critical calibration that is necessary for full interpretation of the seismic data (Moore et al., 1995a; Shipley et al., 1994).

LWD is the most effective tool for measurement of physical properties in poorly consolidated, faulted, and otherwise unstable sediments where standard wireline systems fail. LWD provides measurements from the water line to the bottom of the deepest level of bottom hole assembly penetration. LWD acquires a continuous log of physical properties directly above the drill bit where hole conditions are optimal for logging. LWD measures properties of the formation within a few minutes to less than an hour after cutting the hole, closely approximating in situ conditions.

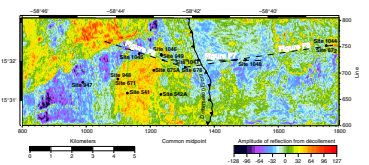
Our LWD transect of the northern Barbados accretionary prism focused on understanding the interrelationships of deformation, fluid flow, seismic imaging, and changes in physical properties (Figs. F2, F3, F4; Frontispiece 2). Changes in physical properties produce seismic reflections; therefore, seismic data provide a direct method to remotely sense physical properties and their evolution as deformation proceeds. However, the physical properties changes producing the reflections need to be calibrated by direct physical measurement to most effectively utilize the seismic data. LWD tools are the best possible means of providing this calibration.

Operations during Leg 171A involved 11 days of continuous LWD operations that primarily occupied areas where previous boreholes had been cored and in which borehole observatories had been placed to monitor temperature and fluid pressure. The five LWD sites drilled during Leg 171A are complemented by two LWD sites drilled during Leg 156 to provide a comprehensive suite of borehole information. This pa-

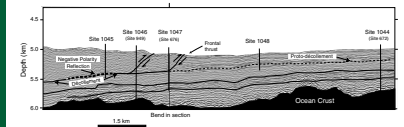
F1. Location map of the Leg 171A area, previous DSDP/ODP legs, and 3-D seismic survey, p. 17.



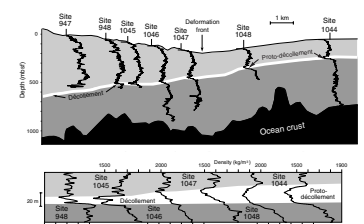
F2. Map of drill site locations and peak seismic amplitude from the proto-décollement zone and décollement zone, p. 18.



F3. Seismic depth section, p. 19.



F4. Generalized cross section through all sites with LWD density data collected during both ODP Legs 156 and 171A, p. 20.



per summarizes the results of Leg 171A and how these data have added value to the previous drilling and seismic reflection studies.

## TECTONIC SETTING OF THE NORTHERN BARBADOS ACCRETIONARY PRISM

The northern Barbados accretionary prism is the leading edge of the Caribbean plate that is being underthrust by the Atlantic Ocean floor at rates estimated at ~3 cm/yr in a westerly to northwesterly direction (Fig. F1) (DeMets et al., 1990; Dixon et al., 1998). The Lesser Antilles to the west defines the volcanic arc, whereas the island of Barbados east of the arc is an outcrop of the forearc accretionary prism. Frontal structures south of the Tiburon Rise include long wavelength folds, widely spaced ramping thrust faults, and extensive reflections from the décollement (Westbrook and Smith, 1983; Bangs and Westbrook, 1991). North of the Tiburon Rise, trench sediment thickness is much thinner and prism thrusts are more closely spaced (Biju-Duval et al., 1982; Westbrook et al., 1984). North of the Tiburon Rise, the Barbados accretionary prism reaches at least 10 km thick and 120 km wide, in addition to a 50-km-wide forearc basin to the west (Bangs et al., 1990; Westbrook et al., 1988). Thus, the accretionary prism forms a wide, low-taper wedge.

## PREVIOUS DRILLING AND SEISMIC REFLECTION STUDIES

DSDP Leg 78A and ODP Legs 110, 156, and 171A focused on the northern flank of the Tiburon Rise. A principal target has been penetration of the décollement zone or plate boundary fault. Here the décollement zone is relatively shallow, and the dominantly hemipelagic-pelagic sedimentary section offers good drilling conditions and good biostratigraphic resolution. This décollement zone (or basal detachment or sole thrust) separates the deformed thrust wedge above from the undeformed sedimentary rocks or basement below (e.g., Twiss and Moores, 1992). Thus, the décollement zone is the surface of maximum structural disharmony beneath the accretionary wedge or prism. We call it the décollement zone because it is of a finite thickness. Structural studies show that the décollement zone becomes better defined in a landward direction and is a shear zone up to 33 m thick at Sites 671 and 948 (Maltman et al., 1997; Shipboard Scientific Party, 1988a; 1995). Anomalies in pore-water chemistry (Gieskes et al., 1990; Kastner et al., 1997) and temperature (Fisher and Hounslow, 1990b) indicate focused fluid along a décollement zone and in subjacent sand layers. Models simulating this fluid expulsion from the prism suggest that the flow is transient (Bekins et al., 1995). The décollement zone is characterized by suprahydrostatic fluid pressures (Labaume et al., 1997; Sreaton et al., 1997; Zwart et al., 1997).

A 3-D seismic reflection survey (Moore et al., 1995a; Shipley et al., 1994) has greatly improved the interpretation of drilling results from the northern Barbados accretionary prism (Figs. F2, F3). The décollement zone commonly coincides with a distinct and locally high-amplitude seismic reflection. Using the 3-D seismic image, the stratigraphic horizon that the décollement zone occupies can be extended seaward, east of the deformation front, as the proto-décollement zone (Fig. F3).

The seismic survey also shows patches of positive and negative seismic polarity in the décollement zone (Fig. F2) (DiLeonardo et al., in press; Shipley et al., 1994). These polarity signatures may signify differing fluid regimes and stress states along the décollement zone (Bangs et al., 1996; Bangs et al., 1999; Shipley et al., 1994; Shipley et al., 1997). Determining the physical properties that define these polarity signatures was a major goal of Leg 171A.

## WHAT DID WE LEARN DURING LEG 171A?

The Leg 171A investigations provided a venue for new investigations and reconsideration of previous interpretations in the context of the new logging data. The site-by-site results and some broader conclusions are documented in the Leg 171A *Initial Reports* volume (Moore et al., 1998a). Results summarized here draw on articles mostly published in the outside literature. The results are presented in three sections: the first focusing on correlations and derived properties of the logs, and the following two sections considering results primarily applicable to areas seaward, or east, of the accretionary prism and to those landward, or west, of the toe of the accretionary prism.

## RESULTS OF LEG 171A: STUDIES FOCUSING ON CORRELATIONS OF LOG-DERIVED PROPERTIES

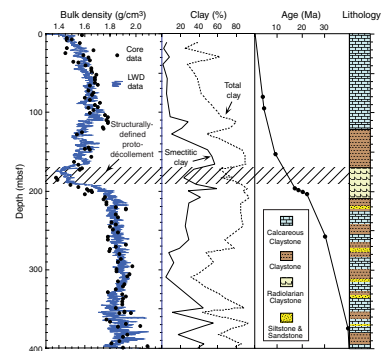
### Definition of Logging Units and Correlation to Lithology

High-quality log data provide an opportunity to evaluate relationships between logging and other rock properties. Multivariate methods of factor and cluster analysis produced fast, reliable, and objective definitions of logging units that correlate well with the lithologic units defined at the cored holes that are adjacent to the Leg 171A sites (Bücker et al., Chap. 2, this volume). Moreover, such objective unit-definition criteria were especially valuable to define log units at Sites 1045 and 1048, where no cores were available.

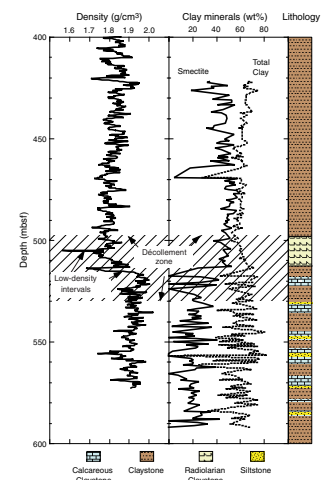
### Correlation of Logs and Seismic Reflection Data

The Leg 171A LWD data immediately showed that the seismically defined décollement zone and proto-décollement zone correlate with a low-density interval in the logs (Fig. F4). The changes in impedance (velocity × density) at the top and bottom of this low-density interval either singularly or in combination result in the seismic reflection that characterized the décollement zone and proto-décollement zone (Bangs et al., 1999). Moreover, this low-density interval correlates with a radiolarian claystone in both the proto-décollement and décollement zones and with the deformed interval of the décollement zone as defined in the cores (Figs. F5, F6). Recognition of these correlations provided a basis for using the seismic data to broadly extend the LWD results and for numerous geologic interpretations of the logging results that are reported below.

F5. Comparison of core bulk density, clay mineralogy, sedimentation rates, structurally defined limits of the proto-décollement zone, and lithology from Site 672 to Site 1044, p. 21.



F6. Comparison of LWD bulk density to clay mineralogy, lithology, and structurally defined limits of the décollement zone at Site 948, p. 22.



The décollement zone is a structural feature of maximum disharmony that can be viewed in cores or in seismic data. In cores, the décollement zone thickness is defined by a zone of concentrated scaly foliation ranging up to 33 m thick (Labaume et al., 1997; Maltman et al., 1997). In seismic reflection images, the thickness of the décollement zone cannot be resolved, although models of the waveforms reflected from the décollement indicate the thickness of the associated low-density interval (see [“Predicting Décollement/Proto-décollement Zone Density and Thickness throughout the Seismic Survey,”](#) p. 8). This low-density zone is not equivalent to the structural décollement and may either encompass the décollement zone where it is developing or be included in the décollement zone where it is more mature and more consolidated (Fig. F6).

### **Velocities Derived from Resistivities**

The Leg 171A LWD data, although of excellent quality, have certain limitations. The LWD tools used during Leg 171A did not include a means of measuring sonic velocity because the available devices are unreliable in sediments with velocities <2000 m/s. The neutron porosity tool is also not effective in high-porosity sediments, and the data we collected was not extensively utilized. Moreover, conversions of LWD density to porosity are hampered by the presence of interlayer water in smectite, which is recorded by the density tool.

To address some of the limitations in the LWD data, Erickson and Jarard (1999) used smectite-corrected, density-based porosities to calibrate a conversion between porosity and formation factor then calculated porosity from resistivity logs. By comparing resistivity-based porosities to velocities from vertical seismic profiles, Erickson and Jarard (1999) estimated velocity profiles for Leg 171A sites. The velocities determined from resistivities can be compared to a wireline velocity log collected during Leg 156 (Shipboard Scientific Party, 1995). Both logs show similar velocities over scales of 10 to 50 m, but the resistivity-velocity log shows much more detailed character, mimicking changes in lithology that were recorded by the resistivity tool and not the wireline sonic velocity tool. Determination of accurate, detailed velocities and porosities from these sediments remains a problem that will hopefully be rectified by improved technology.

## **RESULTS OF LEG 171A: PROCESSES SEAWARD OF THE DEFORMATION FRONT**

### **Origin of Low Density in Proto-décollement Zone**

The distinctly low density of the proto-décollement zone influences the structural evolution both seaward and landward of the deformation front. Options that explain this low density include high radiolarian porosity, low grain density, and overpressuring.

Because the low-density interval at Site 1044 correlates with the upper half of the radiolarian claystone lithology (Fig. F5), we suspected that the cause of the low density was a high proportion of porous radiolarian tests. However, analysis of a series of samples from Site 672 penetrating the proto-décollement zone demonstrated that the radiolarian tests as open pore volumes comprise only 4% to 5% of the proto-décollement section (Wallace, [Chap. 1](#), this volume). The density shift

at the top of the proto-décollement zone is  $-0.12 \text{ g/cm}^3$ . Replacing the sediment matrix with 5% porosity because of radiolarians will only shift the density by  $0.035 \text{ g/cm}^3$  or  $\sim 30\%$  of the observed decrease in density at the top of the proto-décollement zone.

Changes in grain density may also account for part of the density decrease in the proto-décollement zone. The generally high smectite and total clay contents decrease in the downhole transition to the proto-décollement zone (Fig. F5). According to the X-ray diffraction studies (Tribble, 1990), the decrease in smectite and total clays is accounted for by an increase in quartz and feldspar, a shift consistent with the presence of dispersed volcanic ash in this section. Therefore, the low density of the proto-décollement zone cannot be accounted for by an increase in smectite with its internally bound water. However, dispersed volcanic glass (variable but anomalously low grain density) and opal in radiolarians, sponge spicules, and diatoms (grain density of  $2.1 \text{ g/cm}^3$ ) may contribute to the observed density decrease. Because the amount of volcanic glass and opal is undetermined, this idea cannot be explicitly tested.

Finally, the low density and underconsolidation (Taylor and Leonard, 1990) of the proto-décollement zone could be explained by overpressuring. However, a modeling study indicates that the proto-décollement zone should have consolidated given the duration of time since its deposition ( $\sim 20 \text{ m.y.}$ ) and permeabilities of the overlying section (Screaton and Ge, in press). Thus, the maintenance of low density caused by overpressuring is arguable.

In summary, no single factor can adequately explain the origin of the low-density proto-décollement zone. However, the combined effects of radiolarian porosity, low grain density, and overpressuring may combine to account for the observed density minima.

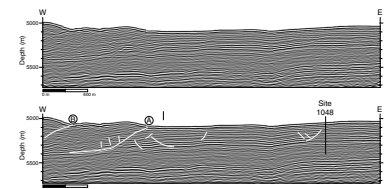
### Deformation in the Proto-décollement Zone and Initiation of the Décollement Zone

The proto-décollement zone was originally defined at Site 672 and correlated to the décollement zone at Site 671 based on lithology, age, and the small-scale faulting and extensional mud-filled veins in lower Miocene radiolarian claystones (Shipboard Scientific Party, 1988b). Shipboard scientists related the deformation at Site 672 to seaward propagation of thrusting from the deformation front, even though this hypothesis seemed mechanically unrealistic.

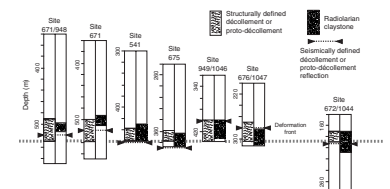
The LWD data indicate that the zone of faulting and veining lies in the zone of low density (Fig. F5). A careful analysis of the 3-D seismic data indicates that small-displacement normal faults sole out at the level of the proto-décollement zone (Fig. F7) (Teas, 1998). This later observation suggests that the proto-décollement zone is inherently weak, predicting the development of the décollement zone in this interval.

Given that the section is relatively uniform claystone above, through, and below the décollement zone, its development in the radiolarian mudstone would not be obviously predicted from lithology alone. The proto-décollement zone (with listric normal faulting) and the décollement zone (with thrusting) are correlated with the low-density radiolarian mudstone (Figs. F5, F6, F8). This low-density interval is most obvious seaward of the deformation front but persists as a residual of two low-density spikes, even at Site 948, farthest landward (Figs. F4, F6). Siliceous sediments are as strong or stronger than clays, so the radi-

F7. East-west seismic section through Site 1048, p. 23.



F8. Correlation of radiolarian claystone and structurally-defined décollement/proto-décollement zone, p. 24.



oliarian lithology offers no strength advantage (Fossum and Fredrich, 1998). However, the lower density and higher porosity is generally correlated with lower strength (Hoshino et al., 1972; Vernik et al., 1993). Therefore, the low density and high porosity of the radiolarian mudstone may account for the localization of failure in this lithology.

The normal faults are common in the section seaward of the deformation front, often sole out in the proto-décollement zone, and arguably disturb the seafloor <800 m from the deformation front (Fig. F7) (Teas, 1998). The latter observation suggests that the normal faulting is young and the compressional state of stress does not propagate far from the limits of the accretionary prism. Such extension may be caused by the flexure of the Tiburon Rise as it approaches the subduction zone. Moreover, incipient thrusting is not known more than several hundred meters seaward of the main frontal thrust (Fig. F7). Thus, any proto-thrust zone is virtually undeveloped at this margin in contrast to Cascadia (Cochrane et al., 1994) or southwest Japan (Morgan and Karig, 1995). The low taper angle of the northern Barbados accretionary prism suggests minimal coupling along the décollement zone (Davis, 1984), which is consistent with the absence of a proto-thrust zone. Simulations of fluid flow from the consolidating accretionary prism and incoming sediment section suggest elevated fluid pressures seaward of the deformation front, which could facilitate faulting of any type (Stauffer and Bekins, in press).

### **Origin of High Heat Flow Seaward of the Deformation Front**

The high heat flow seaward of the deformation front at Site 672 and in surface measurements nearby was explained by fluid flow either along the proto-décollement zone or in sandy turbidites at greater depth (Fisher and Hounslow, 1990a). Anomalously fresh pore water at the level of the sandy turbidites argues for active flow in this interval (Shipboard Scientific Party, 1988b). However, the value of the proto-décollement zone as a conduit transmitting fluid from beneath the accretionary prism has been questioned because (1) the pore-water anomalies at Site 672 are not considered a strong indicator of fluid flow through the proto-décollement zone (Shipboard Scientific Party, 1997), and (2) there is no heat-flow anomaly at Site 543, which is closer to the deformation front but lacks the sandy turbidite section at depth (Tokunaga, in press). The statistical correlation and volumetric strain analysis by Tokunaga (in press) indicates that more rapid consolidation of the mudstones surrounding the sandy turbidites beneath the accretionary prism could account for the fluid sources necessary to produce the heat-flow anomaly at Site 672.

## **RESULTS OF LEG 171A: PROCESSES IN THE DÉCOLLEMENT ZONE**

The décollement zone is a plate boundary fault that initiates at the seaward edge of the accretionary prism and increases in displacement with subduction and evolves into the subduction trace between the North American and Caribbean plates. Studying this fault, therefore, provides unique insights on plate-boundary deformation processes. Critical questions include: What is the nature of this plate boundary

surface? What is the fluid pressure along it? How does it evolve with time? The accessibility of the décollement zone here was the original motivation for the initial DSDP leg (Leg 78A). The décollement zone was not penetrated until ODP Leg 110, and extensive logs through this difficult-to-drill interval were not obtained until the completion of Leg 171A.

### Calibration of the Seismic Reflection from the Décollement Zone

In situ physical properties measurements through the negative-polarity reflections of the décollement zone are critical to calibrate the nature of this reflection. Leg 156 attempted to penetrate and log through a strong negative-polarity reflection at Site 947. This site failed in a zone of hole instability above the décollement zone. Site 1045 was specifically located where the depth to the décollement zone is less than at Site 947, but the negative-polarity reflection remains strong. Site 1045 showed that the low-density interval in the décollement zone correlates with the strong negative-polarity and is probably the most significant result of Leg 171A. This low-density interval is consistent with the low seismic impedance predicted by the waveform modeling (Bangs et al., 1996). This result indicates that the large northeasterly trending negative-polarity area (Shipley et al., 1994) of the décollement zone is also of low density and high porosity.

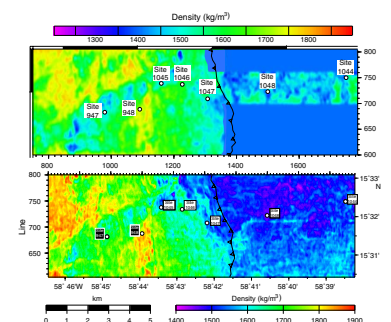
### Predicting Décollement/Proto-décollement Zone Density and Thickness throughout the Seismic Survey

The LWD data constrain density well and therefore allow seismic models that output impedance (velocity  $\times$  density) to be interpreted in terms of density. The seismic data at each drill site can be effectively “forward” modeled using the LWD density distribution and a linear increase in seismic velocity (Bangs et al., 1999). Conversely, modeling or “inversion” of the seismic waveforms everywhere through the décollement zone produces density maps of this surface (Fig. F9) (Bangs et al., 1999; Zhao et al., 2000) that provide a regional basis for interpreting processes in the décollement zone. The above authors have converted the density maps to porosity, but the actual amount of pore water is not exactly known because of the water that remains within the opal and smectite mineral structures (Brown and Ransom, 1996). Therefore, viewing the porosity maps as representative of total water content is more appropriate. Using their inversion of the seismic data, Zhao et al. (2000) also have mapped the thickness of the low-density interval that characterizes the décollement and proto-décollement zones. Figure F4 shows Bangs et al.’s (1999) visualization of the low-density interval associated with the décollement and proto-décollement zones.

### Interpretations of Density Variations

The individual LWD penetrations of the décollement zone plus the density maps produced by the seismic inversions show that the density of the décollement zone increases from the deformation front with depth beneath the accretionary prism (Fig. F9). As the décollement zone densifies, the contrast between it and the immediately overlying accretionary prism is erased. Because the density contrast at the base is

F9. Density maps of the proto-décollement zone and décollement zone produced by inversion of seismic reflection data, p. 25.



larger than at the top, the basal density contrast remains after the overlying contrast is lost. The residual basal density contrast provides a positive impedance contrast that results in the positive seismic reflection that characterized the décollement zone after dewatering.

A northeasterly trending area of reduced density that mimics the area of strong negative polarity (see Figs. F2, F9; Frontispiece 2) is the prominent exception to the trend of densification along the décollement zone west of the deformation front. The penetration at Site 1045 shows that the low-density interval is thinner and slightly higher in density than that observed at either of the sites east of the deformation front. Therefore, the density anomaly in the northeasterly trending area can be interpreted as a residual of the primary density profile. This northeasterly trending area of reduced density is interpreted as an interval of arrested consolidation (Bangs et al., 1999; Moore et al., 1998b; Zhao et al., 2000). The lower density and higher fluid content of this zone requires that the fluid support a greater portion of the overburden than adjacent more dewatered areas. Hence, the area of negative polarity probably has a higher fluid pressure. The occurrence of high amplitude reflections or “bright spots” above the northeasterly trending zone is consistent with leakage of fluids from the zone of negative polarity (and high fluid pressure) into the overlying prism (Shipley et al., 1997; Bangs et al., 1999).

Studies of shear (*S*)-wave velocities and anisotropy suggest that the base of the accretionary prism is underconsolidated (Peacock and Westbrook, in press). The low *S*-wave velocities and high Poisson’s ratios of these sediments near Sites 948 and 949 confirm direct observations of low porosity of the sediments above the décollement zone. *S*-wave splitting studies indicate little alignment in pore space in sediments above the décollement zone, suggesting that the sediment is underconsolidated, not hydrofractured. Underconsolidation above the décollement zone is also indicated by the density distribution at Site 947 and the high-amplitude seismic reflections just above the décollement zone (Bangs et al., 1999).

The arrested consolidation of the décollement zone could be achieved by features that reduce the permeability of the décollement zone conduit or its drainage to adjacent sediments or by enhancement of flow from deep sources. Simulations of bulk density distributions in the décollement zone show that the low-density, apparently arrested consolidation examples can be maintained by reasonable rates of fluid flux from depth (Stauffer and Bekins, in press). Moreover, the documentation of high-angle faults compartmentalizing the décollement zone (DiLeonardo et al., in press) suggests that flow from depth along the décollement zone may be focused laterally and retarded at it updip termination, helping to arrest consolidation.

A popular previous view interpreted the northeasterly area of negative-polarity seismic reflections and low density as hydrofractures created by true physical dilation and superlithostatic fluid pressures (Bangs et al., 1996; Brown et al., 1994; Shipley et al., 1994; Moore et al., 1995b). Extensional veins in the décollement zone (Labaume et al., 1997; Vrolijk and Sheppard, 1991) indicate localized extensional fractures that could lower the impedance. However, the fact that the LWD densities in the décollement zone at Site 1045 are slightly higher than that at the reference sites argues against dilation and hydrofracture. Because the density is measured ~40 min after the hole is cut, some have argued that density values lower than those measured may have been eliminated as a result of the collapse of the hydrofractures. However,

the seismic inversions (Bangs et al., 1999; Zhao et al., 2000) indicate that the density in the areas of negative-polarity reflections in the décollement zone is higher everywhere than the density in the protodécollement zone. This observation supports the view that the negative-polarity reflections are explained by arrested consolidation, not hydrofracture.

In summary, we favor the interpretation of the northeasterly-trending zone of negative polarity as a result of arrested consolidation, as it represents a simpler interpretation of the available data than the dilative hydrofracture option.

### **Causes of Densification in the Décollement Zone**

Processes that may cause the systematic densification of the décollement zone (Fig. F9) include collapse of radiolarian porosity, collapse of intergranular porosity at all scales, cementation, and mineral phase transitions.

Analysis of the radiolarian porosity shows that it is largely gone because of the physical collapse of the radiolarians, infilling tests with authigenic mineral phases, and dissolution of tests for décollement zone sediments at Sites 671 and 948, the farthest west penetration of the décollement zone (Wallace and Moore, unpubl. data; T. Steiger, pers. comm., 1998; Ogawa, 1993). However, as the radiolarian porosity averages only ~5% in the incoming section, its complete destruction contributes little to the overall densification of the décollement zone (Wallace and Moore, unpubl. data). More significantly, scanning electron microscope (SEM) studies indicate a significant decrease in intergranular porosity due to the collapse of clay mineral fabric, which can account for 65% to 90% of the observed density change (Wallace and Moore, unpubl. data).

Densification caused by phase changes occurs because of the loss of interlayer water in smectite, phase changes in opal fossil tests, and precipitation of zeolites. Experiments suggest that the smectite in the décollement zone is dewatering to some degree (Fitts and Brown, 1999), and X-ray diffraction studies suggest that the opal is transforming to opal-CT and quartz in the décollement zone (T. Steiger, pers. comm., 1998). Zeolites also fill radiolarian tests and are in the clay matrix (Wallace and Moore, unpubl. data). All of the above processes densify the décollement zone but are less important than the collapse of intergranular porosity between clay-sized particles.

### **Causes of Localization of the Décollement Zone**

We believe that the décollement zone initiates in the radiolarian mudstone because it is of low density and, therefore, weaker than adjacent sediments (Fig. F5). However, densification with underthrusting eliminates any preferential weakness caused by low density. The correlation of the décollement zone and radiolarian mudstone is strong, as viewed in the drill holes (Fig. F8) and, arguably, can be continued beyond the boreholes with the seismic reflection data (Wallace and Moore, unpubl. data). If the décollement zone densifies with underthrusting, then why does it remain localized?

Experiments with clays indicate they decrease in strength from 25% to 75% of their peak shear strength because of the orientation of the platy clay minerals (Lupini et al., 1981). SEM images of the décollement zone document well the zonal orientation of clay minerals (Labaume et

al., 1997; Wallace and Moore, unpubl. data). Thus, this strain-softening phenomena in clays apparently overcomes any tendency toward increased strength caused by low density. Moreover, any overpressuring of the décollement zone associated with its localized fluid flow would weaken it and favor its persistence. Finally, even though the décollement zone densifies, the sediments surrounding it also densify, tending to partially perpetuate the relatively low density of the décollement zone.

### **Décollement Zone Permeability**

Leg 171A resulted in an unanticipated measurement of permeability over the 45 m separating Sites 1046 and 949 (Screaton et al., in press). Site 949, with a previously installed borehole monitoring system (CORK), showed a pressure response caused by LWD packer tests at Site 1046. Modeling of this response yields a permeability of  $10^{-14}$  m<sup>2</sup>, which is 1–2 orders of magnitude higher than that expected from previous single-hole operations at Site 949. This two-hole measurement is considered robust; if it is representative of the entire décollement zone, then the décollement zone could drain fluid at the rate that it is produced (Screaton et al., in press). Although the measurement may correctly represent the permeability in the vicinity of Site 1046, continuing densification with underthrusting or compartmentalization of the décollement zone by high-angle faulting (DiLeonardo et al., in press) may account for a further decrease in décollement zone permeability.

## **SUMMARY OF LWD RESULTS PERTINENT TO ACCRETIONARY PRISM EVOLUTION**

1. The décollement zone develops in a low-density interval in the sedimentary section incoming to the subduction zone. Initiation of the décollement zone in this interval is apparently caused by its low strength, in part because of its low density.
2. The low density of the proto-décollement zone makes it the weak sole fault for listric normal faults in the incoming sedimentary section.
3. The transition from extension (normal faulting) to compression is virtually at the toe of the accretionary prism, indicating that compressional stresses are not propagated far seaward of the accretionary prism.
4. High heat flow seaward of the accretionary prism is explained by fluid flow in the subjacent sand layers, not in the proto-décollement zone.
5. With underthrusting beneath the accretionary prism, the décollement zone densifies in a patchy manner, primarily because of the collapse of clay mineral fabric. The one area penetrated by LWD with retarded densification corresponds to negative-polarity seismic reflections in the décollement zone.
6. The density data from the LWD holes allow a confident inversion of the seismic data for density along the proto-décollement zone and décollement zone.
7. The strong negative-polarity reflections in the décollement zone indicate areas of arrested consolidation, not hydrofracture. These areas of arrested consolidation represent fluid compart-

ments in the décollement zone and are locally bounded by high-angle faults. The areas of arrested consolidation may represent channels of focused fluid flow from depth, which tends to retard consolidation.

8. The drilling results and, arguably, the seismic reflection data indicate the décollement zone remains localized in an interval of radiolarian claystone. Weakening of this smectite-rich lithology during shear explains the tendency of the décollement zone to remain localized in its initial position.
9. During LWD operations, an inadvertent two-hole hydrologic test indicated significantly higher permeability of a scale of 45 m more than was previously inferred from single borehole tests.

## **ACKNOWLEDGMENTS**

The accomplishments of Leg 171A depended on a flexible ODP science structure that allowed the minileg and provided the extra resources necessary for the LWD program. Success of the operations at sea depended on the reliable, high-quality instruments provided by Anadrill-Schlumberger and its dedicated engineers. Additionally, the ship's crew, the drilling crew, and the ODP technical support staff provided unfailing assistance. Moore acknowledges the USSAC for funds to support the preparation of this article and NSF grant OCE 9618166 for support of the analysis of the seismic reflection data reported. Moore acknowledges Landmark Graphics Corporation for providing seismic processing and interpretation software that was both taken to sea during Leg 171A and later used to create the images of seismic reflection data included in this chapter. Comments by Adam Klaus and Rich Jarrard improved the scientific content and presentation of this manuscript.

## REFERENCES

- Bangs, N.L., Shipley, T.H., Moore, J.C., and Moore, G., 1999. Fluid accumulations and channeling along the Northern Barbados Ridge décollement thrust. *J. Geophys. Res.*, 104: 20399–20414.
- Bangs, N.L.B., Shipley, T.H., and Moore, G.F., 1996. Elevated fluid pressures and fault zone dilation inferred from seismic models of the northern Barbados Ridge décollement. *J. Geophys. Res.*, 101:627–642.
- Bangs, N.L.B., and Westbrook, G.K., 1991. Seismic modeling of the décollement zone at the base of the Barbados Ridge accretionary complex. *J. Geophys. Res.*, 96:3853–3866.
- Bangs, N.L.B., Westbrook, G.K., Ladd, J.W., and Buhl, P., 1990. Seismic velocities from the Barbados Ridge Complex: indicators of high pore fluid pressures in an accretionary complex. *J. Geophys. Res.*, 95:8767–8782.
- Bekins, B.A., McCaffrey, A.M., and Driess, S.J., 1995. Episodic and constant flow models for the origin of low-chloride waters in a modern accretionary complex. *Water Resour. Res.*, 31:3205–3215.
- Biju-Duval, B., LeQuellec, P., Mascle, A., Renard, V., and Valery, P., 1982. Multibeam bathymetric survey and high resolution seismic investigations of the Barbados Ridge complex (Eastern Caribbean): a key to the knowledge and interpretation of an accretionary wedge. *Tectonophysics*, 86:275–304.
- Biju-Duval, B., Moore, J.C., et al., 1984. *Init. Repts. DSDP*, 78A: Washington (U.S. Govt. Printing Office).
- Brown, K.M., Bekins, B., Clennell, B., Dewhurst, D., and Westbrook, G., 1994. Heterogeneous hydrofracture development and accretionary fault dynamics. *Geology*, 22:259–262.
- Brown, K.M., and Ransom, B., 1996. Porosity corrections for smectite-rich sediments: impact on studies of compaction, fluid generation, and tectonic history. *Geology*, 24:43–84.
- Cochrane, G.R., MacKay, M.E., Moore, G.F., and Moore, J.C., 1994. Consolidation and deformation of sediments at the toe of the central Oregon accretionary prism from multichannel seismic data. In Westbrook, G.K., Carson, B., Musgrave, R.J., et al., *Proc. ODP, Init. Repts.*, 146 (Pt. 1): College Station, TX (Ocean Drilling Program), 421–426.
- Davis, D.M., 1984. The compressive mechanics of accretionary wedges applied to the Leg 78A study area near Barbados. In Biju-Duval, B., Moore, J.C., et al., *Init. Repts. DSDP*, 78A: Washington (U.S. Govt. Printing Office), 569–579.
- Demets, C., Gordon, R.G., Argus, D.F., and Stein, S., 1990. Current plate motions. *Geophys. J. Int.*, 101:425–478.
- DiLeonardo, C.G., Moore, J.C., Nissen, S.E., and Bangs, N.L., in press. Control of internal structure and fluid migration pathways within the Barbados Ridge décollement zone by strike-slip faulting: evidence from coherence and 3-D seismic amplitude imaging. *Geol. Soc. Am. Bull.*
- Dixon, T.H., Farina, F., DeMets, C., Jansma, P., Mann, P., and Calais, E., 1998. Relative motion between the Caribbean and North American plates and related boundary zone deformation from a decade of GPS observations. *J. Geophys. Res.*, 103:15157–15182.
- Erickson, S.N., and Jarrard, R., 1999. Porosity-formation factor and porosity-velocity relationships in the Barbados prism. *J. Geophys. Res.*, 104:15391–15408.
- Fisher, A.T., and Hounslow, M.W., 1990a. Heat flow through the toe of the Barbados accretionary complex. In Moore, J.C., Mascle, A., et al., *Proc. ODP, Sci. Results*, 110: College Station, TX (Ocean Drilling Program), 345–363.
- , 1990b. Transient fluid flow through the toe of the Barbados accretionary complex: constraints from Ocean Drilling Program Leg 110 heat flow studies and simple models. *J. Geophys. Res.*, 95:8845–8858.

- Fitts, T., and Brown, K., 1999. Stress-induced smectite dehydration: ramifications for patterns of freshening and fluid expulsion in the N. Barbados accretionary wedge. *Earth Planet. Sci. Lett.*, 172:179–197.
- Fossum, A.F., and Fredrich, J.T., 1998. Estimation of constitutive parameters for the Belridge Diatomite, South Belridge Diatomite Field. *Sandia Nat. Lab. [Tech. Rep.] SAND*, SAND98–1407.
- Gieskes, J.M., Vrolijk, P., and Blanc, G., 1990. Hydrogeochemistry of the northern Barbados accretionary complex transect: Ocean Drilling Program Leg 110. *J. Geophys. Res.*, 95:8809–8818.
- Hoshino, K., Koide, H., Inami, K., Iwamura, S., and Mitsui, S., 1972. Mechanical properties of Japanese Tertiary sedimentary rocks under high confining pressures. *Chishitsu Chosajo [Geol. Surv. Jpn.]*.
- Kastner, M., Zheng, Y., Laier, T., Jenkins, W., and Ito, T., 1997. Geochemistry of fluids and flow regime in the décollement zone at the northern Barbados Ridge. In Shipley, T.H., Ogawa, Y., Blum, P., and Bahr, J.M. (Eds.), *Proc. ODP, Sci. Results*, 156: College Station, TX (Ocean Drilling Program), 311–319.
- Labaume, P., Kastner, M., Trave, A., and Henry, P., 1997. Carbonate veins from the décollement zone at the toe of the northern Barbados accretionary prism: microstructure, mineralogy, geochemistry, and relations with prism structures and fluid regime. In Shipley, T.H., Ogawa, Y., Blum, P., and Bahr, J.M. (Eds.), *Proc. ODP, Sci. Results*, 156: College Station, TX (Ocean Drilling Program), 79–96.
- Lupini, J.F., Skinner, A.E., and Vaughan, P.R., 1981. The drained residual strength of cohesive soils. *Geotechnique*, 31:181–213.
- Maltman, A., Labaume, P., and Housen, B., 1997. Structural geology of the décollement at the toe of the Barbados accretionary prism. In Shipley, T.H., Ogawa, Y., Blum, P., and Bahr, J.M. (Eds.), *Proc. ODP, Sci. Results*, 156: College Station, TX (Ocean Drilling Program), 279–292.
- Masle, A., Moore, J.C., et al., 1988. *Proc. ODP, Init. Repts.*, 110: College Station, TX (Ocean Drilling Program).
- Moore, G.F., Zhao, Z., Shipley, T.H., Bangs, N., and Moore, J.C., 1995a. Structural setting of the Leg 156 area, northern Barbados Ridge accretionary prism. In Shipley, T.H., Ogawa, Y., Blum, P., et al., *Proc. ODP, Init. Repts.*, 156: College Station, TX (Ocean Drilling Program), 13–27.
- Moore, J.C., Klaus, A., Bangs, N.L., Bekins, B., Bücker, C.J., Brückmann, W., Erickson, N.E., Horton, T., Ireland, P., Major, C.O., Peacock, S., Saito, S., Sreaton, E.J., Shimeld, J.W., Stauffer, P.H., Taymaz, T., Teas, P.A., and Tokunaga, T., 1998a. Consolidation patterns during initiation and evolution of a plate-boundary décollement zone: Northern Barbados accretionary prism. *Geology*, 26:811–814.
- Moore, J.C., Klaus, A., et al., 1998b. *Proc. ODP, Init. Repts.*, 171A: College Station, TX (Ocean Drilling Program).
- Moore, J.C., Shipley, T.H., Goldberg, D., Ogawa, Y., Filice, F., Fisher, A., Jurado, M.-J., Moore G.F., Rabaute, A., Yin, H., Zwart, G., and Brueckmann, W., Henry, P., Ashi, J., Blum, P., Meyer, A., Housen, B., Kastner, M., Labaume, P., Laier, T., Leitch, E.C., Maltman, A.J., Peacock, S., Steiger, T.H., Tobin, H.J., Underwood, M.B., Xu, Y., Zheng, Y., 1995b. Abnormal fluid pressures and fault zone dilation in the Barbados accretionary prism: evidence from logging while drilling. *Geology*, 23:605–608.
- Morgan, J.K., and Karig, D.E., 1995. Décollement processes at the Nankai accretionary margin, Southeast Japan. *J. Geophys. Res.*, 100:15221–15231.
- Ogawa, Y., 1993. Destruction and dissolution of radiolarian tests in relation to the present and ancient décollement zones, Barbados accretionary complex, Ocean Drilling Program Leg 110. *Sci. Rep. Inst. Geosci., Univ. Tsukuba*, 14 (Sect. B):53–64.
- Peacock, S., and Westbrook, G.K., in press. Shear-wave velocities and anisotropy in the Barbados accretionary complex. *J. Geophys. Res.*
- Sreaton, E.J., Carson, B., Davis, E., and Becker, K., 2000. Permeability of a décollement zone: results from a two-well experiment in the Barbados accretionary complex. *J. Geophys. Res.*, 105: 21403–21410.

- Screaton, E.J., Fisher, A.J., Carson, B., and Becker, K., 1997. Barbados Ridge hydrogeologic tests: implications for fluid migration along an active décollement. *Geology*, 25:239–242.
- Screaton, E.J., and Ge, S., in press. Anomalous high porosities in the proto-décollement of the Barbados accretionary complex: do they indicate overpressures? *Geophys. Res. Lett.*
- Shipboard Scientific Party, 1988a. Site 671. In Mascle, A., Moore, J.C., et al., *Proc. ODP, Init. Repts.*, 110: College Station, TX (Ocean Drilling Program), 67–204.
- , 1988b. Site 672. In Mascle, A., Moore, J.C., et al., *Proc. ODP, Init. Repts.*, 110: College Station, TX (Ocean Drilling Program), 205–310.
- , 1995. Site 948. In Shipley, T.H., Ogawa, Y., Blum, P., et al., *Proc. ODP, Init. Repts.*, 156: College Station, TX (Ocean Drilling Program), 87–192.
- , 1998. Site 1044. In Moore, J.C., Klaus, A., et al., *Proc. ODP, Init. Repts.*, 171A: College Station, TX (Ocean Drilling Program), 19–37.
- Shipley, T.H., Moore, G.F., Bangs, N.L., Moore, J.C., and Stoffa, P.L., 1994. Seismically inferred dilatancy distribution, northern Barbados Ridge décollement: implications for fluid migration and fault strength. *Geology*, 22:411–414.
- Shipley, T.H., Moore, G.F., Tobin, H.J., and Moore, J.C., 1997. Synthesis of the Barbados décollement seismic reflection response from drilling-based geophysical observations and physical properties. In Shipley, T.H., Ogawa, Y., Blum, P., and Bahr, J.M. (Eds.), *Proc. ODP, Sci. Results*, 156: College Station, TX (Ocean Drilling Program), 293–302.
- Shipley, T.H., Ogawa, Y., Blum, P., et al., 1995. *Proc. ODP, Init. Repts.*, 156: College Station, TX (Ocean Drilling Program).
- Stauffer, P., and Bekins, B., in press. Consolidation modeling of the Northern Barbados décollement. *J. Geophys. Res.*
- Taylor, E., and Leonard, J., 1990. Sediment consolidation and permeability at the Barbados forearc. In Moore, J.C., Mascle, A., et al., *Proc. ODP, Sci. Results*, 110: College Station, TX (Ocean Drilling Program), 289–308.
- Teas, P.A., 1998. The effect of relatively small scale structural features on fluid flow, fluid entrapment, and tectonic dewatering [Ph.D. thesis]. Univ. California Santa Cruz.
- Tokunaga, T., 2000. The role of turbidites on compaction and dewatering of the underthrust sediments: new evidence from logging while drilling, ODP Leg 171A. *Earth Planet. Sci. Lett.*, 178: 385–395.
- Tribble, J.S., 1990. Clay diagenesis in the Barbados accretionary complex: potential impact on hydrology and subduction dynamics. In Moore, J.C., Mascle, A., et al., *Proc. ODP, Sci. Results*, 110: College Station, TX (Ocean Drilling Program), 97–110.
- Twiss, R.J., and Moores, E.M., 1992. *Structural Geology*: New York (Freeman).
- Underwood, M.B., and Deng, X., 1997. Clay mineralogy and clay geochemistry in the vicinity of the décollement zone, northern Barbados Ridge. In Shipley, T.H., Ogawa, Y., Blum, P., and Bahr, J.M. (Eds.), *Proc. ODP, Sci. Results*, 156: College Station, TX (Ocean Drilling Program), 3–30.
- Vernik, L., Bruno, M., and Bovberg, C., 1993. Empirical relations between compressive strength and porosity of siliciclastic rocks. *Int. J. Rock Mech. Min. Sci.*, 30:677–680.
- Vrolijk, P., and Sheppard, S.M.F., 1991. Syntectonic carbonate veins from the Barbados accretionary prism (ODP Leg 110): record of paleohydrology. *Sedimentology*, 38:671–690.
- Westbrook, G.K., Ladd, J.W., Buhl, P., Bangs, N., and Tiley, G.J., 1988. Cross section of an accretionary wedge: Barbados Ridge complex. *Geology*, 16:631–635.
- Westbrook, G.K., Mascle, A., and Biju-Duval, B., 1984. Geophysics and structure of the Lesser Antilles forearc. In Biju-Duval, B., Moore, J.C., et al., *Init. Repts. DSDP, 78A*: Washington (U.S. Govt. Printing Office), 23–38.

- Westbrook, G.K., and Smith, M.J., 1983. Long décollements and mud volcanoes: evidence from the Barbados Ridge Complex for the role of high pore-fluid pressure in the development of an accretionary complex. *Geology*, 11:279–283.
- Zhao, Z., Moore, G., Bangs, N.L., and Shipley, T.H., 2000. Spatial variations of the décollement/proto-décollement zone and their implications: a 3-D seismic inversion study of the Northern Barbados accretionary prism. *Island Arc*, 9:219–236.
- Zwart, G., Brückmann, W., Moran, K., MacKillop, A.K., Maltman, A.J., Bolton, A., Vrolijk, P., Miller, T., Gooch, M.J., and Fisher, A., 1997. Evaluation of hydrogeologic properties of the Barbados accretionary prism: a synthesis of Leg 156 results. *In* Shipley, T.H., Ogawa, Y., Blum, P., and Bahr, J.M. (Eds.), *Proc. ODP, Sci. Results*, 156: College Station, TX (Ocean Drilling Program), 303–310.

Figure F1. Location map of the Leg 171A area, previous DSDP/ODP legs, and 3-D seismic survey (black box). Shaded area represents Barbados accretionary prism. The accretionary prism is divided into northern and southern parts at about 15°N, where the Tiburon Rise impinges on the prism. Arrow indicates direction of convergence of the North American plate relative to the Caribbean plate ( $28 \pm 6$  mm/yr along  $N78W \pm 18^\circ$ ) (Dixon et al., 1998). Depths are in meters.

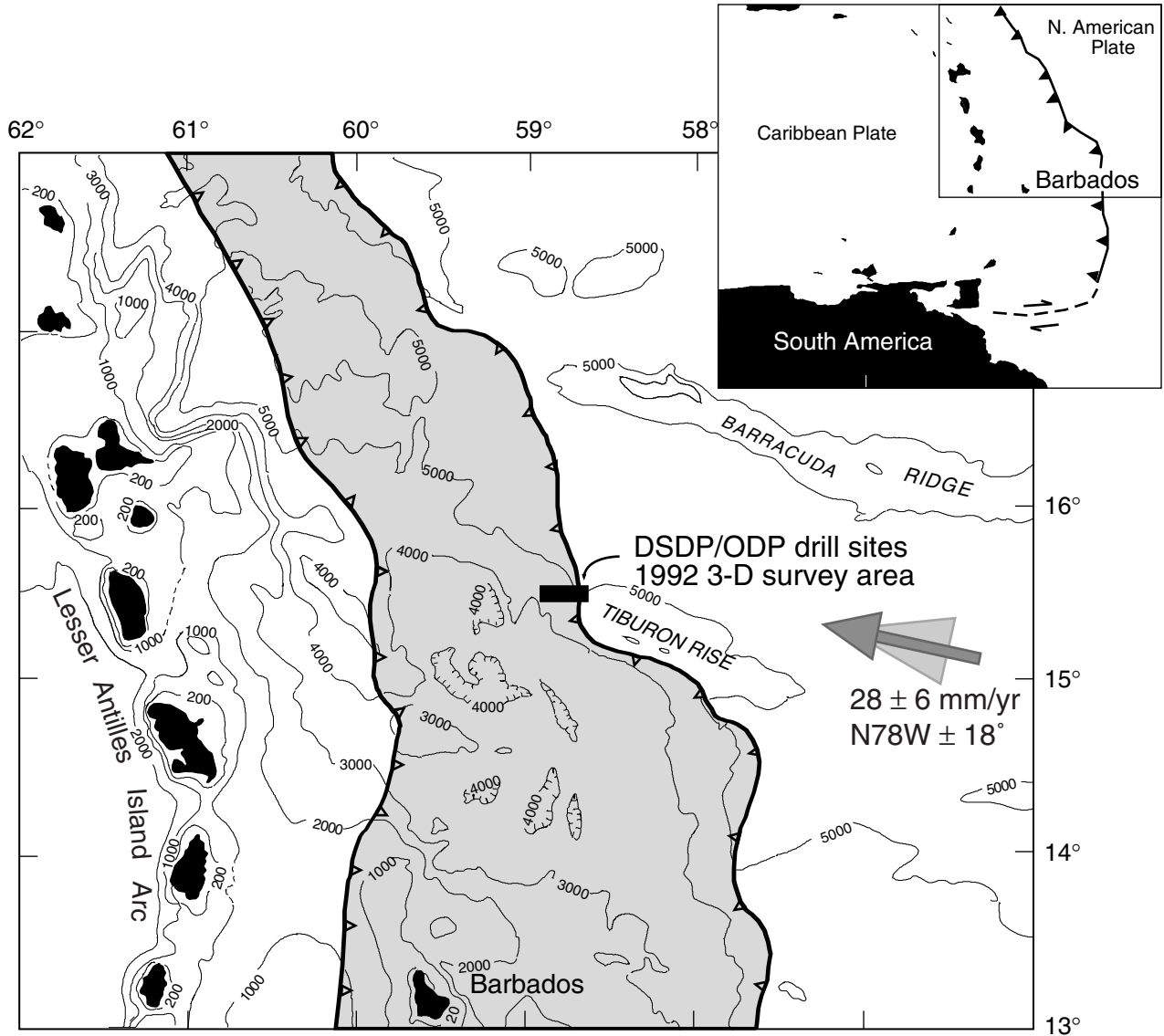


**Figure F2.** Map of drill site locations and peak seismic amplitude from the proto-décollement zone and décollement zone in the eastern portion of the 3-D seismic volume (DiLeonardo et al., in press). Note the northeasterly trending area of negative polarity beneath the accretionary prism. This area is interpreted as a conduit for migration of fluid from depth. Dashed lines show locations of seismic data in Figures F3, p. 19, and F7, p. 23. (See also [Frontispiece 2.](#))

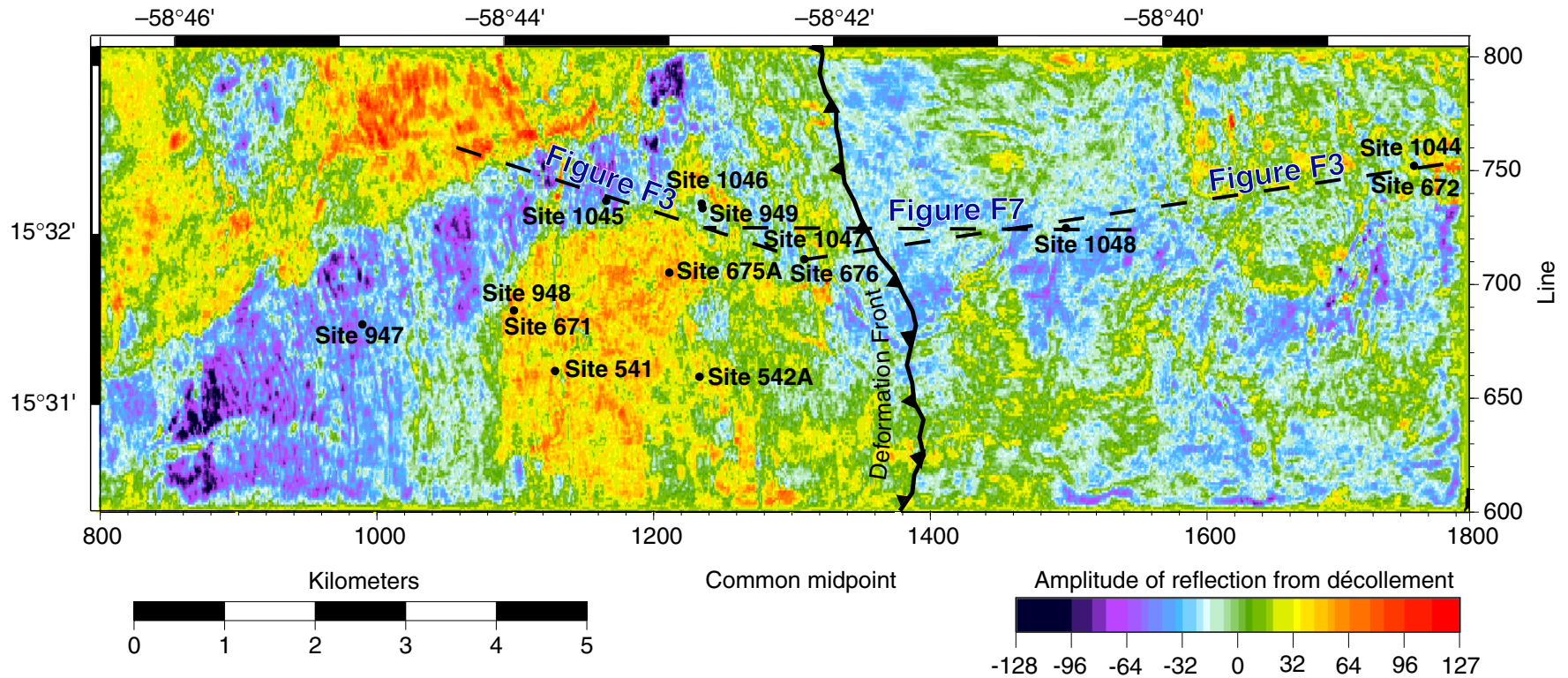


**Figure F3.** Seismic depth section extending from west of Site 1045 to Sites 676 and 1047 then to Sites 672 and 1044. Solid lines below the level of the décollement zone and proto-décollement zone show approximate limits of the sandy underthrust terrigenous sequence. This sandy sequence may be the zone that migrates warm fluids from beneath the accretionary prism, which generates the observed heat-flow anomaly seaward of the deformation front. See Figure F2, p. 18, for location of the seismic section.

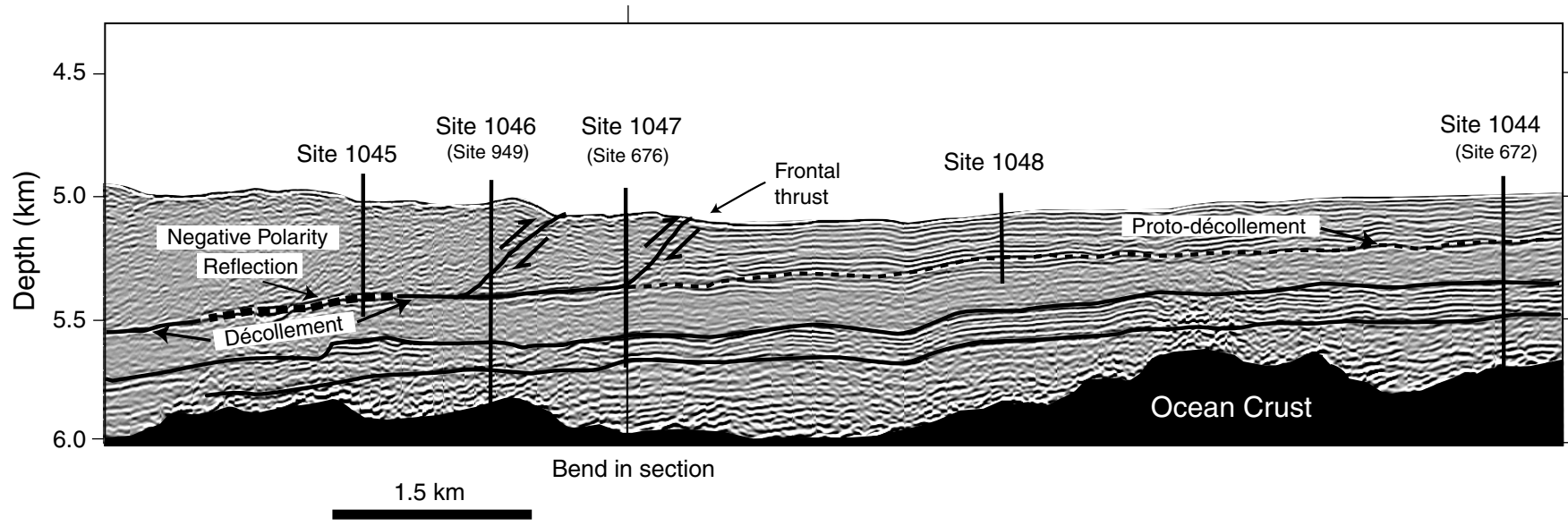


**Figure F4.** Generalized cross section through all sites with LWD density data collected during both ODP Legs 156 and 171A (Bangs et al., 1999). The lighter and upper shaded area of both figure panels represents the accretionary prism and the equivalent sediments in the incoming sedimentary section. The darker and lower shaded area of both figure panels indicates the portion of the sedimentary section being underthrust and its equivalent seaward of the deformation front. The lighter area separating the shaded areas is the low-density interval that is associated with the décollement zone and proto-décollement zone. It is not equivalent in thickness to the structurally defined décollement or proto-décollement but may encompass or be included in them. Depth scales on both upper and lower panels indicate relative, not absolute, depth.

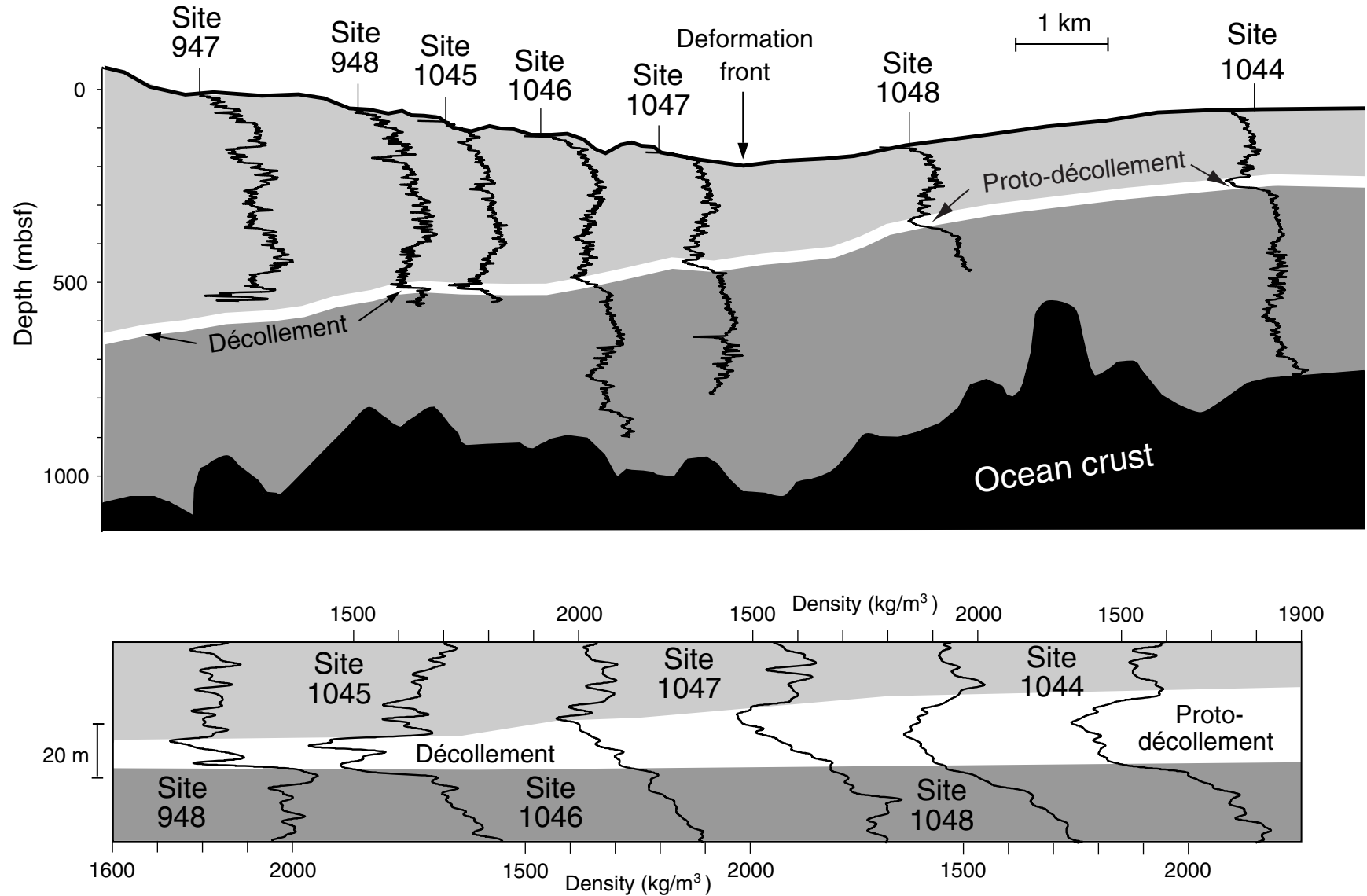


Figure F5. Comparison of core bulk density, clay mineralogy, sedimentation rates, structurally defined limits of the proto-décollement zone, and lithology from cores at Site 672 to LWD bulk density at colocated Site 1044 (Shipboard Scientific Party, 1988b; Tribble, 1990). Note the correlation of the low-density interval in the density curve with the proto-décollement zone and the radiolarian claystone.

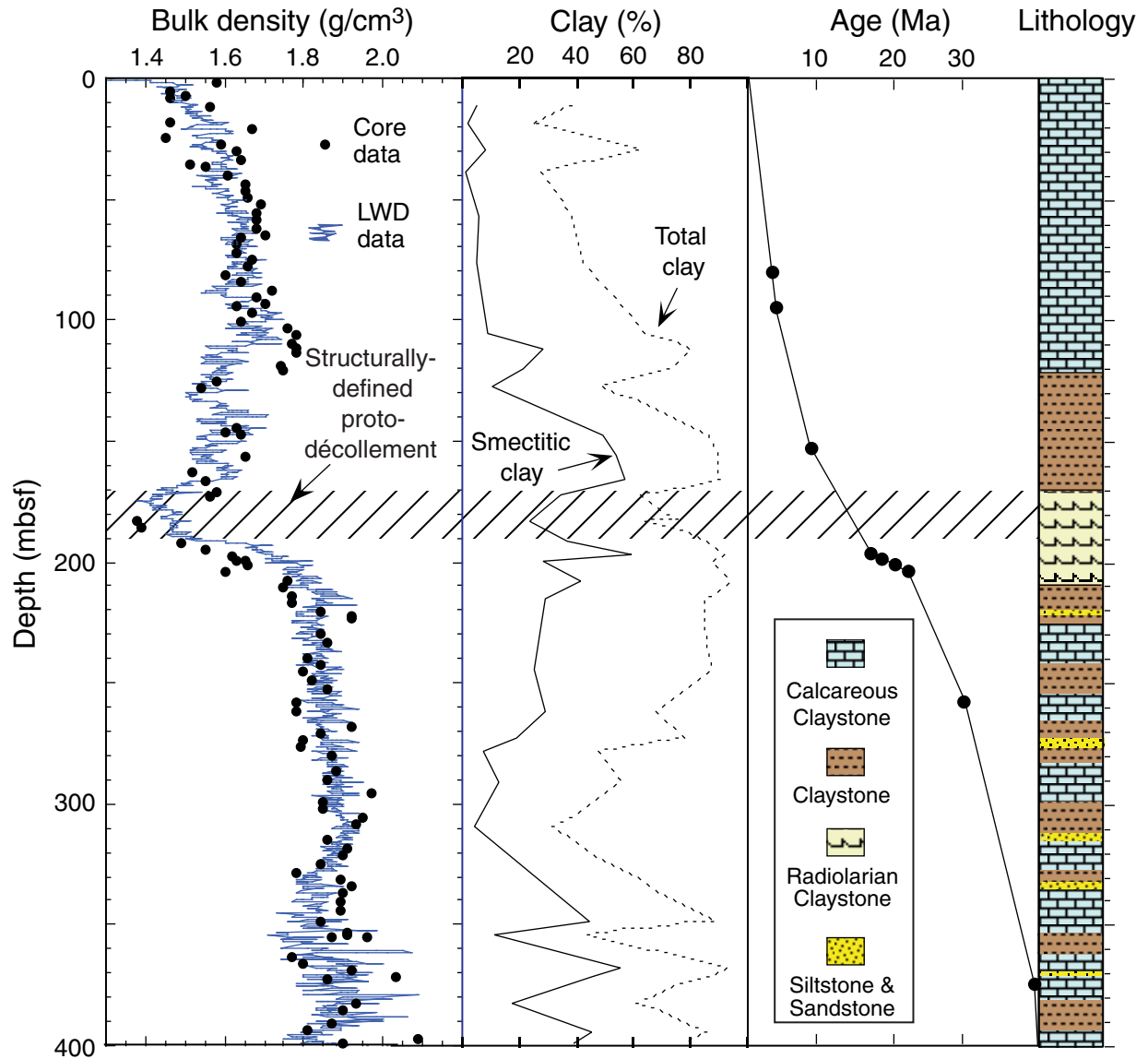
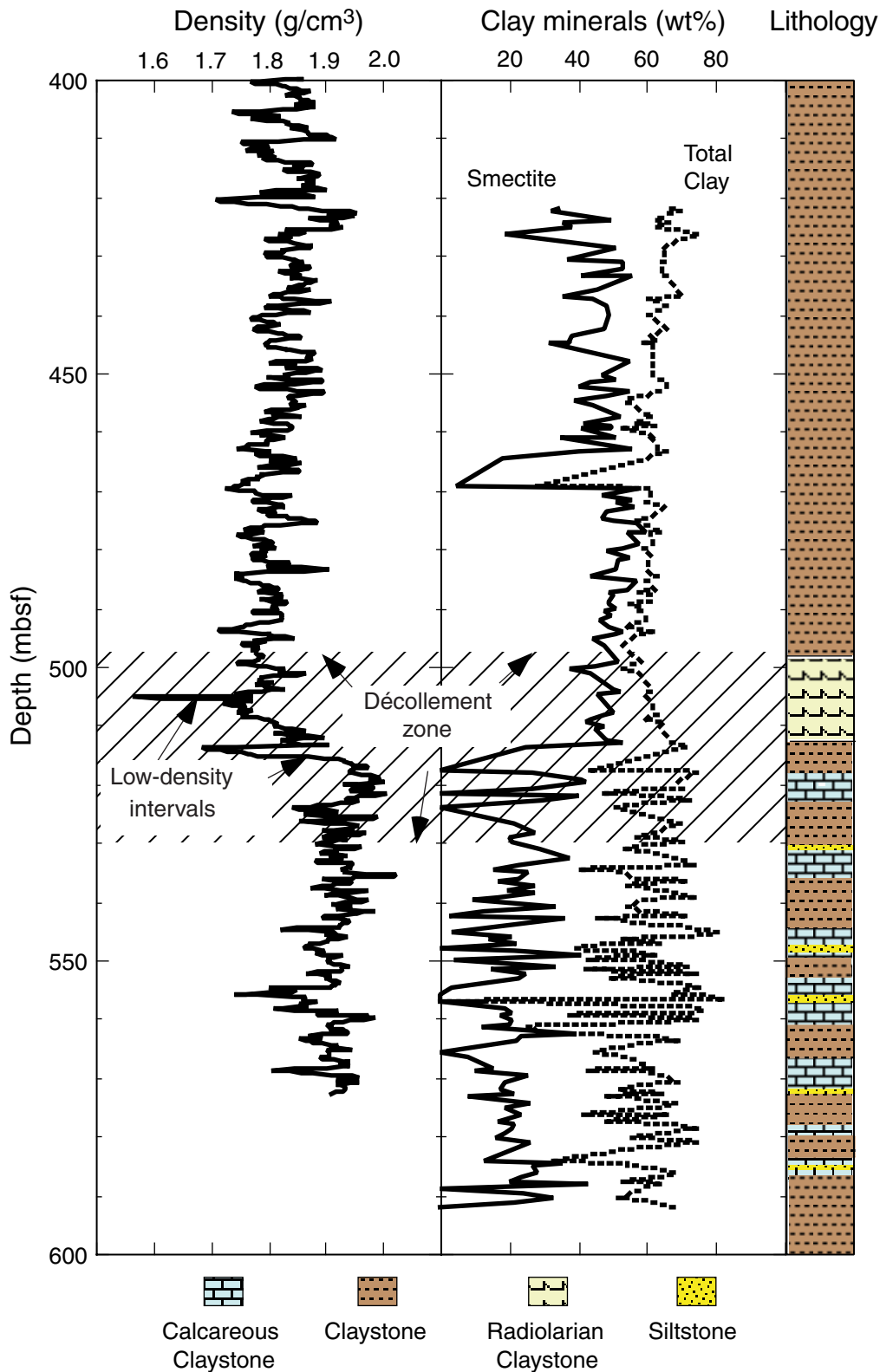
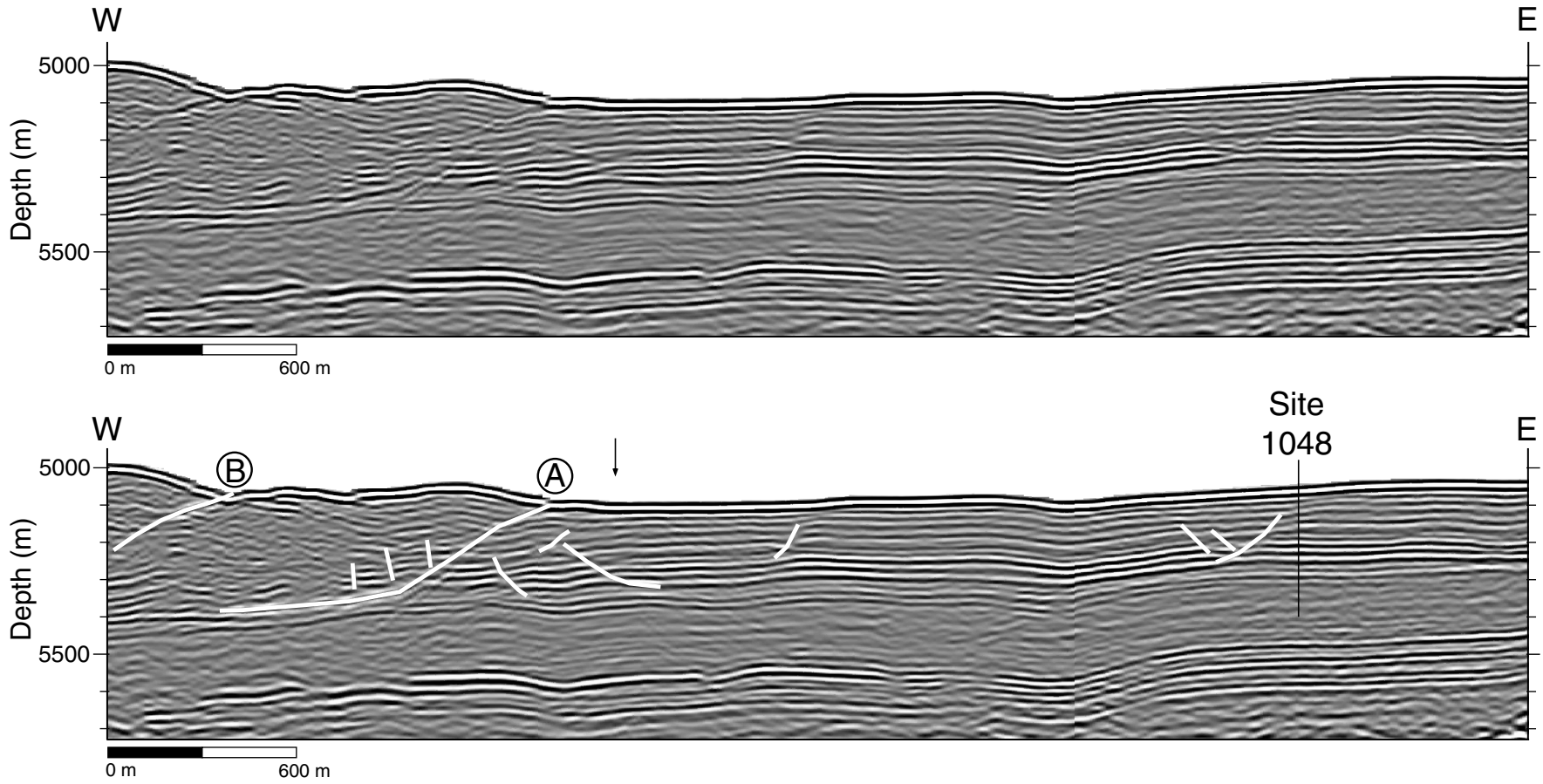


Figure F6. Comparison of LWD bulk density to clay mineralogy, lithology, and structurally defined limits of the décollement zone at Site 948 (Shipboard Scientific Party, 1995; Underwood and Deng, 1997). This site is the locality farthest west of the deformation front that still penetrates the décollement zone. Note that the décollement zone still includes two low-density intervals that are interpreted as remnants of a former thick, low-density interval as seen in Figure F5, p. 21. Also note that the décollement zone here has thickened to 33 m and includes all of the radiolarian claystone lithology.



**Figure F7.** East-west seismic section through Site 1048. A listric normal fault west of Site 1048 soles into the proto-décollement zone. A second listric normal fault (below arrow) is near the deformation front of the prism and strikes parallel to the front. Circled letters A and B indicate prominent in-sequence thrust faults. Note the steeply dipping reverse faults above the frontal thrust ramp. Figure modified from Teas (1998).



**Figure F8.** Correlation of radiolarian claystone and structurally-defined décollement/proto-décollement zone (Wallace and Moore, unpubl. data) as designated by shipboard sedimentologists and structural geologists (Biju-Duval and Moore, 1984; Mascle et al., 1988; Shipley et al., 1995) and décollement/proto-décollement zone reflection from seismic data. Note that the stratigraphic columns at each hole are aligned on the base of the décollement zone (heavy gray dashed line) as determined from cores. The zone reflection is the position of the peak amplitude of the waveform, and its depth is measured from the peak amplitude of the water-bottom reflection.

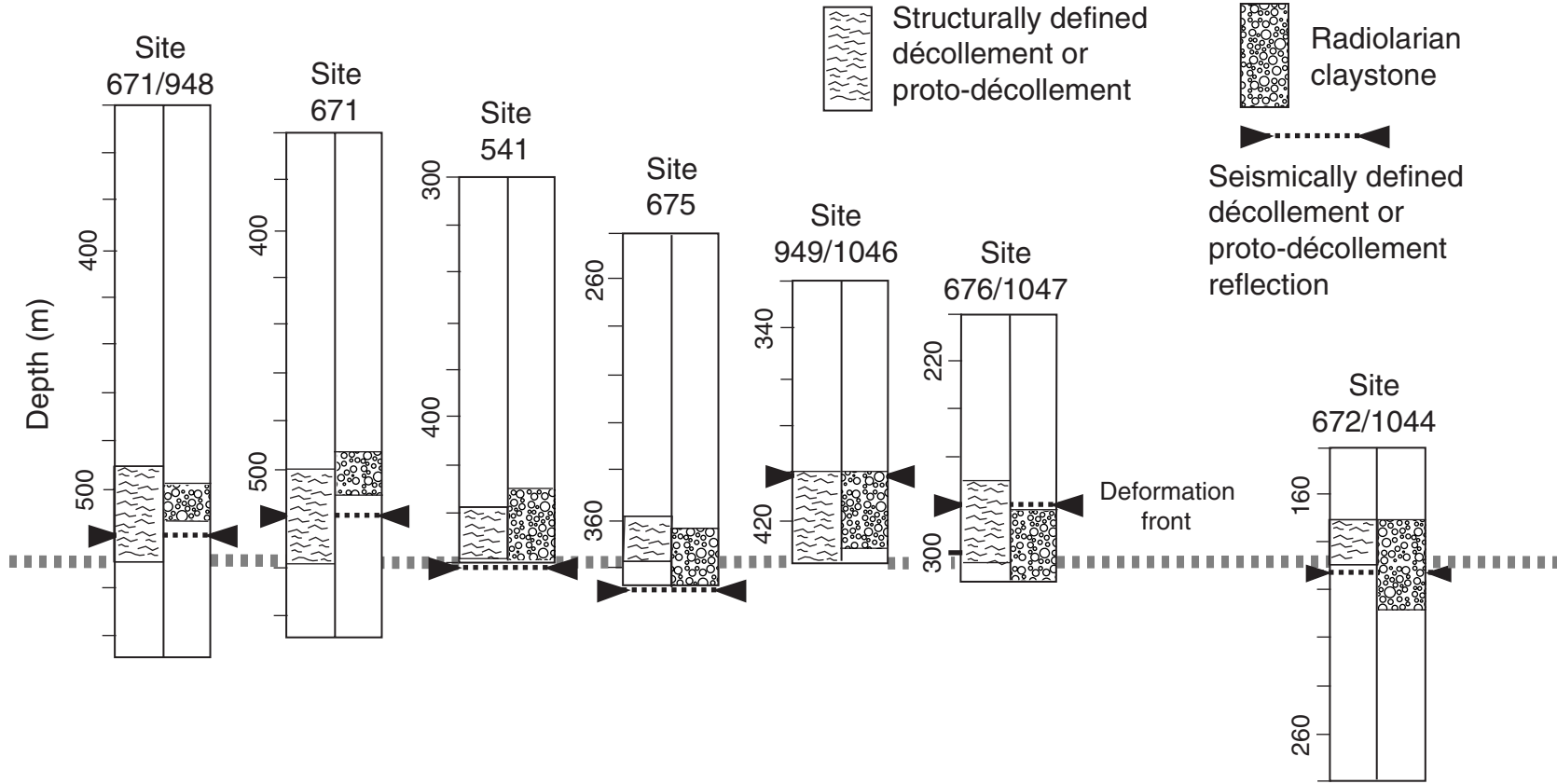


**Figure F9.** Density maps of the proto-décollement zone and décollement zone produced by inversion of seismic reflection data. Upper panel from Bangs et al. (1999) and lower panel from Zhao et al. (2000). Note that both show an overall increase in density with underthrusting west of the deformation front and a northeasterly trending area of reduced density beneath the accretionary prism west of the deformation front. The lower panel provides complete coverage of the proto-décollement zone and shows an increase in density to the south in the proto-décollement zone. Distance scales are equivalent, but note that separate density scales apply to the upper and lower panels of the diagram. (See also [Frontispiece 2.](#))

